An Alternative Approach to Spectrum-Based Atherosclerotic Plaque Characterization Techniques Using Intravascular Ultrasound (IVUS) Backscattered Signals

Amin Katouzian[1], Babak Baseri[1], Elisa E. Konofagou[1,2], and Andrew F. Laine[1,2]

[1] Biomedical and [2] Radiology Departments, Columbia University, NY USA
{ak2432,laine}@columbia.edu

Abstract. In this paper, the discrete wavelet packet frames are used to delineate the atherosclerotic plaque components using intravascular ultrasound (IVUS) backscattered signals. The frames are classified in an unsupervised fashion deploying K-means clustering technique and the generated prognosis histology (PH) images are quantified using relative histology images. While existing tissue characterization algorithms fail to differentiate between blood and plaque signals, the proposed algorithm can be used to estimate the lumen border at higher levels of wavelet expansion. We will demonstrate the in-vitro and in-vivo tissue characterization as well as lumen border detection results employing 40 MHz rotating unfocused single-element transducers. It is concluded that our two dimensional (2-D) algorithm, which is independent of the cardiac and catheter motions, performs well in both in-vivo and in-vitro cases.

Keywords: Wavelet Packets, Atherosclerotic Plaque Characterization, Intravascular Ultrasound (IVUS).

1 Introduction

Cardiac catheterization supplemented with IVUS is often used in routine interventional procedures to investigate the sides of stenosis throughout the artery in addition to angiogram. The IVUS not only provides the 2-D gray scale cross sectional images of the arterial wall and atherosclerosis but also its radiofrequency (RF) signals can be further processed to characterize the plaque constitutes. The ultimate goal of such characterization is: 1) to detect the vulnerable plaques, 2) to study the progression or regression of the plaques subject to treatment approach. Although there are different definitions for plaque vulnerability by different histopathologists, we will justify our results with the one introduced in [1].

Real time acquisition, sufficient signal penetration and low cost image formation and acquisition techniques/instruments make IVUS superior to other imaging modalities to date. Accordingly, researchers have developed IVUS-based algorithms using different techniques such as elastography [2], integrated backscatter (IB) coefficients [3] and spectral analysis [4]. The later has been implemented in the

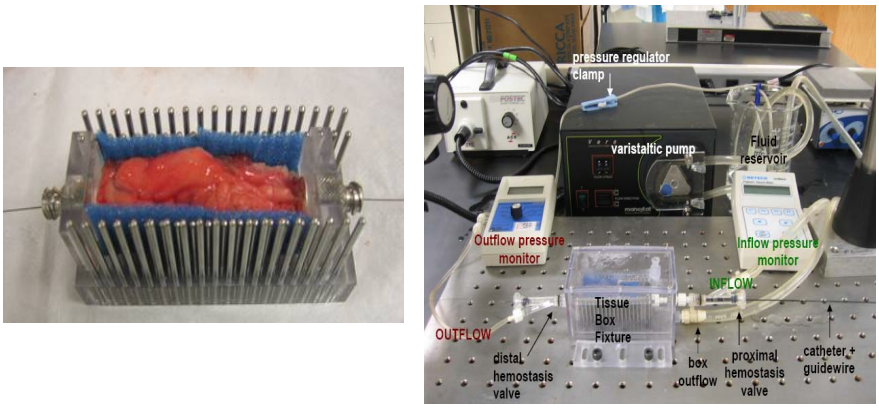

(a) (b)

Fig.1. Tissue cage fixture (a), experiment setup (b).

VOLCANO (Rancho Cordova, CA) IVUS clinical scanners using 20 MHz 64 elements phased array transducers. It has been shown that the variability among extracted spectral features using 8-features algorithm and transducer's spectral parameters (bandwidth, center frequency) make the classification challenging [5].

This motivated us to develop a texture-based algorithm using discrete wavelet packet frame (DWPF) and 2-D envelope detection method based on the work by authors in [6]. The extracted textural features are perfectly suited for classification and capture characteristics of the plaque with the highest correlation to histology. This would resolve one of the main current limitations of IVUS, which is discrimination between fibrotic and lipidic tissues [7].

2 In-vitro Data Collection

We collected the hearts from two sources; autopsy and transplant surgery, within 24 hours postmortem. The arteries were dissected from the hearts with approximate size of $20-60\times 20\times 20\,\mathrm{mm}^2$ $(l\times w\times h)$. We tied off the major branches, attached the endplates to the distal and proximal ends, and placed the segment into a tissue cage fixture, Fig. 1(a). Circulating phosphate buffered saline (PBS) was used to ensure constant pressure (100 mmHg) as well as flow and to maintain the artery physiologically open at 37° Celsius, Fig. 1(b). The 40 MHz Atlantis Boston Scientific (Fremont, CA) IVUS catheter was introduced and advanced on a $0.014''$ guide wire and a complete automatic pullback was performed from the distal to proximal side. The RF data was collected using two 12-bit Acqiris boards (Monroe, NY) and digitized at periodic time intervals, $T_s = 2.5ns\left(f_s = 400MHz\right)$. The catheter pullback speed and the frame rate were set to 0.5 mm/s and 30 frames/s, respectively. After imaging, the artery was pressure fixed with 10% buffered formaldehyde under 100

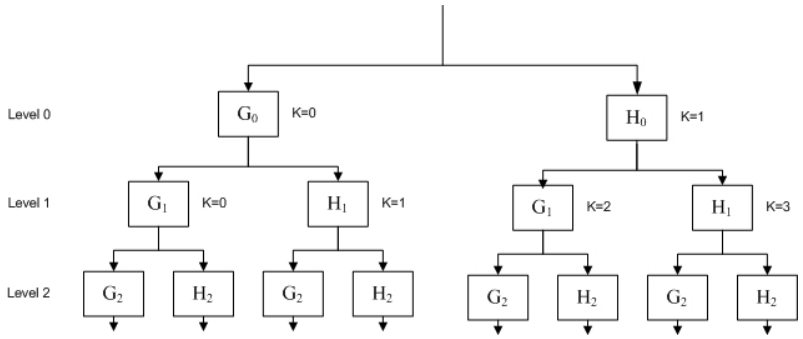

Fig. 2. Tree structure for discrete wavelet packet frames (DWPF) and associate indexes.

mmHg for three hours followed by decalcification. The histology blocks were sectioned from distal to proximal every 2mm (corresponding to 120 frames of the IVUS pullback) using the side rods. Blocks were then embedded in paraffin. For each block, three sections were used for histology. The first two sections were stained with hematoxylin and eosin (H&E) and Movat Pentachrome, and the last section was kept unstained for future necessary staining (e.g., Sirus Red).

3 Methods

Discrete wavelet packet transform (DWPT) [8] is the over complete version of the decomposition process in the discrete wavelet transform (DWT) [9-10], in which every generated coefficient in the decomposition tree is passed through high-pass and low-pass filters. The cost of such a generalization is an increased in computational complexity. Unlike the DWT and DWPT, the decompositions are translation invariant in DWPF and no decimation occurs between levels (Fig. 2). This makes the DWPF superior in algorithms used for texture segmentation. Since the IVUS signals are sampled at the rate of f_s, it is more appropriate to consider the discrete signals that can be represented by a set of wavelets packet coefficients at the first level $(l = 0)$. For the tree-structured scheme demonstrated in Fig. 2, we can write:

$$S_{2k}^{l+1}(\omega) = G_l(\omega) S_k^l(\omega),\ S_{2k+1}^{l+1}(\omega) = H_l(\omega) S_k^l(\omega) \qquad (1)$$

where ω represents the radian frequency and $S_k^l(\omega)$ is the Fourier transform of the frame coefficients at channel k and level l.

3.1 Filter Bank Specification

The high-pass $G_l(\omega)$ and low-pass $H_l(\omega)$ filters at level l, as described in [8], can be written as follows:

$$H_l(\omega) = H_0\left(2^l \omega\right), G_l(\omega) = G_0\left(2^l \omega\right) \qquad (2)$$

Consequently, the multi-channel wavelet schematic in Fig. 2 behaves like a filter bank with channel filters:

$$\left\{F_k^l(\omega) \middle| 0 \le k \le 2^l - 1\right\} \qquad (3)$$

where $F_k^l(\omega)$ can be derived recursively as follows:

$$F_0^0(\omega) = G_0(\omega), F_1^0(\omega) = H_0(\omega) \qquad (4)$$

$$F_{2k}^{l+1}(\omega) = G_{l+1}(\omega) F_k^l(\omega) = G_0\left(2^{l+1}\omega\right) F_k^l \qquad (5)$$

$$F_{2k+1}^{l+1}(\omega) = H_{l+1}(\omega) F_k^l(\omega) = H_0\left(2^{l+1}\omega\right) F_k^l \qquad (6)$$

It has been shown that the selection of the filters $G_0(\omega)$ and $H_0(\omega)$ can have significant impact on the texture classification performance [6]. The filter candidates must satisfy crucial criteria such as symmetry as well as boundary accuracy and have optimal frequency response. Hence, we selected Lemarie-Battle [10] wavelets, that are symmetric (have linear phase response) and quadrature mirror filters (QMF). The former property alleviates boundary effects through simple methods of mirror extension. The wavelets using QMF, as well as constructed filter bank $F_k^l(\omega)$ cover exactly the frequency domain and satisfy the property:

$$\left|G_0(\omega)\right|^2 + \left|H_0(\omega)\right|^2 = \left|G_0(\omega)\right| + \left|H_0(\omega)\right| = 1 \qquad (7)$$

$$\sum_{k=0}^{2l-1} \left|F_k^l(\omega)\right|^2 = \sum_{k=0}^{2l-1} \left|F_k^l(\omega)\right| = 1 \qquad (8)$$

3.2 Feature Extraction

The features were extracted by processing the IVUS signals for every frame in (r, θ) domain. Each frame contains 256 lines that span 360 degree with 2048 samples per line. In order to have an optimized frame size in respect to the computational complexity and the textural resolution, we interpolated (spline) and decimated the signals in the lateral and axial directions by factor of 2 and 4, respectively to generate

the square M=512 pixels frame. For each IVUS frame, a tensor product extension was used in which the channel filters were denoted by $F_{i\times j}^{l}(\omega_r,\omega_\theta)=F_i^l(\omega_r)F_j^l(\omega_\theta)$. Consequently, such an extension will lead to the orientation selectivity in the decomposition tree. Four possible orientations can be considered excluding the root node, which is omnidirectional:

1. The node last filtered by $G_l(\omega_r)H_l(\omega_\theta)$ corresponds to the vertical orientation. The highpass filter G_l and lowpass filter H_l are applied in the axial and lateral directions, respectively.
2. The node last filtered by $H_l(\omega_r)G_l(\omega_\theta)$ corresponds to the horizontal orientation. The lowpass filter H_l and highpass filter G_l are applied in the axial and lateral directions, respectively.
3. The node last filtered by $G_l(\omega_r)G_l(\omega_\theta)$ corresponds to the diagonal orientation. The highpass filter G_l is applied in the axial and lateral directions, respectively.
4. The node last filtered by $H_l(\omega_r)H_l(\omega_\theta)$ has the same orientation as its parent. The lowpass filter H_l is applied in the axial and lateral directions, respectively.

Finally, the envelope of the signals was computed and the feature matrix was constructed as follows:

$$\vec{V}_{i,j}=\left\{e_{k,i,j}^{l}\,\middle|\,0\le k\le\left(2^{l-1}\right),i,j=1,...,M\right\} \qquad (9)$$

where $e_{k,i,j}^{l}$ represents the envelope value of pixel (i,j) for the k-th components at level l.

3.3 Classification

The overall justification of in-vivo real-time plaque characterization is performed by the interventional cardiologists through the use of classified tissues. For this reason, we chose the k-means clustering algorithm in order to classify the extracted features and generate the prognosis histology (PH) images. We utilized the unsupervised classifier to quantify the reliability of the extracted signatures. Our hypothesis is that if the classification results (PH images) driven by the unsupervised signatures preserve their high correlation with the histology images used here as ground truth, then the features can be used reliably in the training data set for supervised classification. We have categorized plaque components into four classes $(N_c=4)$ i.e., lipidic, fibrotic, calcified and background (no tissue).

For every representation matrix $X_{M\times M}$ a label was assigned to each pixel by modulo N_c. We computed the center of clusters $\left\{\vec{C}_\kappa\,\middle|\,0\le\kappa\le N_c-1\right\}$ by calculating the mean vector for each class. The pixel $\left\{x_{i,j}\,\middle|\,i,j=1,...,M\right\}$ was assigned to the class κ if the Euclidean distance between the corresponding pixel and the class center

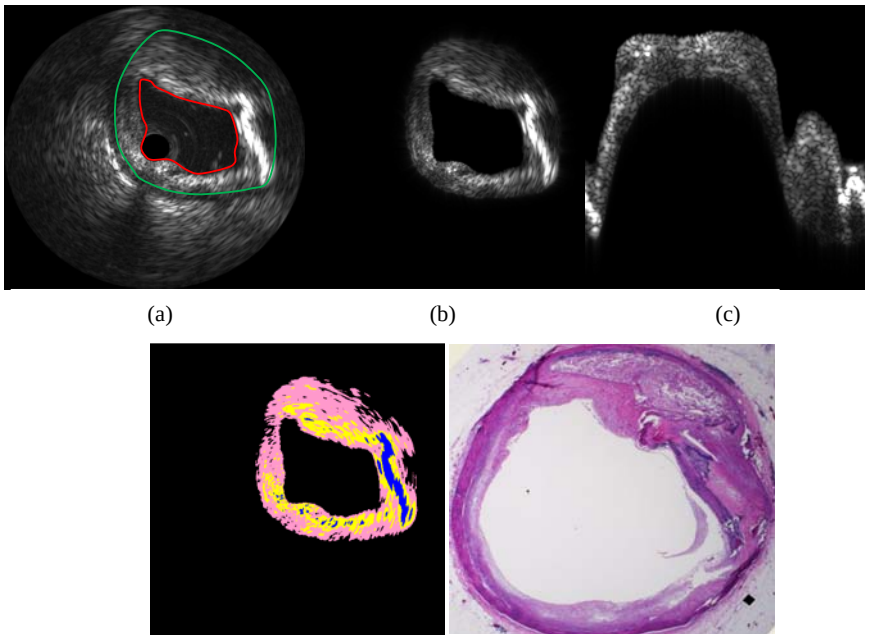

(a) (b) (c)

(d) (e)

Fig. 3. IVUS image with manually traced vessel wall (green) and lumen (red) borders (a), segmented plaque in Cartesian coordinates (b), segmented plaque in (r,θ) coordinates (c), generated PH image (pink, yellow and blue represent lipidic, fibrotic and calcified components, respectively) (d), Movat Pentachrome histology image (e)

$\vec{C}_\kappa$ was the closest. The centers of the clusters were updated in an iterative fashion by recomputing the relative mean vectors. The procedure was terminated once no change in labeling occurred.

4 Experimental Results and Quantification

Sixty four cross-sections of interest (CSI) collected from 32 cadaver hearts, including 26 left anterior descending (LAD), 28 right coronary artery (RCA) and 20 left circumflex (LCX) segments that had more than 30% stenosis. As we mentioned in the preceding section, we decimated the signals and used spline interpolation to generate 512-by-512 scan converted (Cartesian domain) B-mode images. For each frame, an expert manually segmented the plaque by tracing the vessel wall and lumen borders, Fig. 3(a). The corresponding plaque signals were read and saved in a matrix with the same size of IVUS image in the (r,θ) domain, Fig. 3(c).

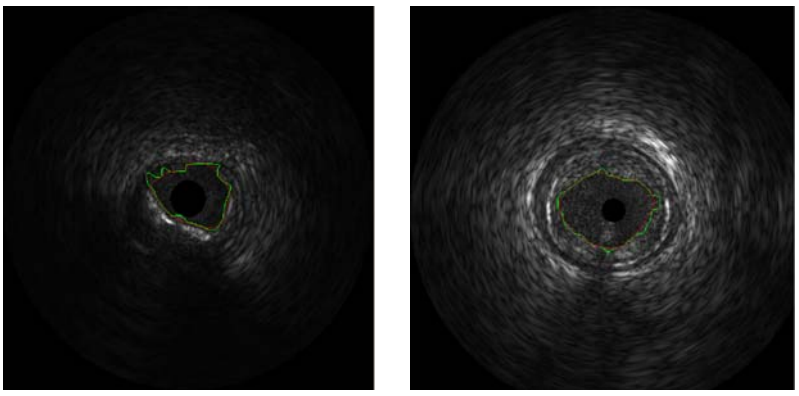

(a) (b)

Fig. 4. Automated detected lumen contour (green) by the algorithm using Lemarie-Battle filters of order 18, expansion level L=4, number of classes N_c=2 and manually traced contour (red) by and expert. In-vivo (a), In-vitro using circulating human blood (b)

We performed our algorithm on 512-by-512 matrices and selected Lemarie-Battle filters of order 18, decomposition level $L = 2$ and number of classes $N_c = 4$. Finally, the resulting classified images were mapped onto Cartesian plane, Fig. 3(d). Fig. 3 demonstrates a CSI, corresponding Movat Pentachrome histology image, and the PH image. The blue, yellow and pink colors exhibit calcified, fibrotic, and lipidic plaque components, respectively. Two independent histopathologists evaluated the results contrasting the histology images corresponding to the PH images. The accuracy of classified tissues was found to be 81.71%, 82.76% and 85.51% for fibrotic, lipidic and calcified components, respectively. The accuracy of IVUS-VH technique using autoregressive (AR) analysis in combination with a classification tree for 30 MHz single element transducers has been reported to be 90.4%, 92.8%, 90.9% and 89.5% for the training data set and 79.7%, 81.2%, 92.8% and 85.5% for the test dataset in fibrotic, fibro-lipidic, calcified and calcified necrotic regions, respectively.

As we mentioned in Section 1, none of the existing algorithms is capable of characterizing the atherosclerotic tissues and differentiate between blood and plaque signals (estimate the lumen border). We evaluated the algorithm performance on lumen border estimation using 18 in-vivo CSI collected from three patients and 14 in-vitro CSI collected from two cadaver hearts. Fig. 4 demonstrates the automatic detected lumen contours (green) and the manually traced contours (red) by an expert for both cases. Our results show that the manual and automated detected lumen borders are correlated very well $\left(r = 0.9854, y = 0.953x + 0.725\right)$, Fig. 5(a). We also computed the Tanimoto coefficient $\left(\eta\right)$, Fig. 5(b), to measure how well the automated detected contour is matched with corresponding manually traced contour:

$$\eta = \frac{N_c^{contour}}{N_a^{contour} + N_m^{contour} - N_c^{contour}} \qquad (10)$$

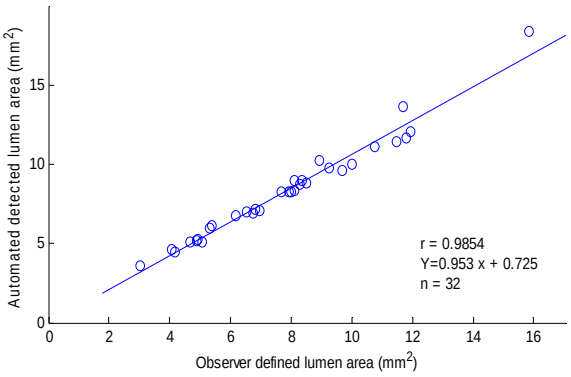

(a)

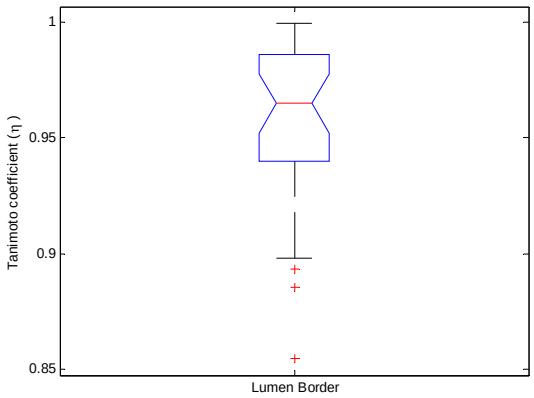

(b)

Fig. 5. Comparison of automated detected lumen area and expert-defined lumen area (a), Box-Whisker plot of Tanimoto coefficients of lumen border.

5 Summary and Conclusion

In this paper, we presented a reliable two 2-D texture-derived atherosclerotic tissue characterization algorithm as an alternative to spectrum-based approaches like IV-VH, IB-IVUS and full-spectrum analysis. We processed the IVUS signals for each frame and extracted the textural features by using multi-channel wavelet packet analysis. The wavelet packet signatures were classified in an unsupervised fashion using K-means clustering algorithm.

The main advantage of the proposed algorithm is that it can reliably classify tissues regardless of the transducer center frequency or spectrum while inconsistency among the spectrum-derived features within the transducer's bandwidth still remains a major challenge. However, we were not able to detect the necrotic core components directly. Although both necrotic core tissues and lipid-rich pools have been recognized as markers for detection of vulnerable plaques, it is an advantage to have a classification algorithm that is able to detect the necrotic core in addition to fibrotic, lipidic and calcified tissues. In the future, we will attempt to extend the algorithm to supervised classification on raw IVUS backscattered signals and investigate this issue.

We will focus on two important aspects in future studies. First, the effects of blood on generated PH images and classification performance will be considered. In fact, it is an inevitable step to validate the reliability of the in-vitro trained classifier for in-vivo atherosclerotic plaque characterization. Secondly, the feasibility of tissue classification within the regions of acoustic shadowing behind calcification will be tested. It has been reported that the tissue characterization in these regions remains difficult [11]. Our hypothesis was that sufficient spectral features would not exist due to signal attenuation in the densely calcified regions. This can be investigated through our proposed technique, since the background (no tissue) had been considered as one of the classes. We will test the tissue characterization and lumen border detection performance using mechanically rotating single-element 40 MHz Atlantis Boston scientific and 45 MHz Revolution Volcano catheters in future studies.

Acknowledgement

We wish to express our sincere appreciations to Dr. Stephane Carlier for his invaluable support. We thank Boston Scientific Corporation (Fremont, CA) for providing us the 40 MHz acquisition system. We also thank Jennifer Lisauskas and Dr. Stephen Sum, at InfraRedx (Burlington, MA), who developed the artery fixation cage and their help in collecting IVUS data is acknowledged. The histology samples were processed at CVPath (Gaithersburg, MD) under supervision of Dr. R. Virmani.

References

1. Virmani, R., Burke, A. P., Kolodgie, F. D., Farb, A.: Pathology of the thin-cap fibroatheroma: A type of vulnerable plaque. J. Inteven. Cardiol., vol. 16, No. 3, pp. 267-272 (2003)
2. Korte, C. L., van der Steen, A. F. W., Cespedes, E. I., Pasterkamp, G., Carlier, S. G., Mastik, F., Schoneveld, A. H., Serruys, P. W., Bom, N.: Characterization of plaque components and vulnerability with intravascular ultrasound elastography. Physics in Med. & Biol. vol. 45, pp. 1465-1475 (2000)
3. Kawasaki, M., Takatsu, H., Noda, T., Sano, K., Ito, Y., Hayakawa, K., Tsuchiya, K., Arai, M., Nishigaki, K., Takemura, G., Minatoguchi, S., Fujiwara, T., Fujiwara, H.: In Vivo Quantitative Tissue Characterization of Human Coronary Arterial Plaques by Use of Integrated Backscatter Intravascular Ultrasound and Comparison With Angioscopic Findings. Circulation, pp. 2487- 2492, May (2002)

4. Nair., A., Kuban, B. D., Obuchowski, N., Vince, D. G.: Assessing spectral algorithms to predict atherosclerotic plaque composition with normalized and raw intravascular ultrasound data. Ultrasound in Med. & Biol., vol. 27, no. 10, pp. 1319–1331 (2001)
5. Katouzian, A., Sathyanarayana, S., Baseri, B., Konofagou, E. E., Carlier, S. G.: Challenges in Atherosclerotic Plaque Characterization with Intravascular Ultrasound (IVUS): From Data Collection to Classification. IEEE Trans. on Information Technology in Biomedicine, vol. 12, no. 3, pp. 315-327 (2008)
6. Laine, A. F., Fan, F.: Frame representation for texture segmentation. IEEE Trans. Image Proc., vol. 5, no. 5, pp. 771-780 (1996)
7. Hiro, T., Leung, C. Y., De Guzman, S., Caiozzo, V. J., Fervid, A. R., Karimi, H., Helfant, R. H., Tobis, J. M.: Are soft echoes really soft? Intravascular ultrasound assessment of mechanical properties in human atherosclerotic tissue. American Heart J. vol. 133, pp. 1-7 (1997)
8. Coifman, R.R., Wickerhauser, M.V.: Entropy-based algorithms for best basis selection. IEEE Trans. Inform. Theory, pt. II, vol. 38, no. 2, pp. 713-718, Mar. (1992)
9. Rioul, O.: A discrete-time multiresolution theory. IEEE Trans. Sig. Proc., vol. 41, no. 8, pp. 2591-2606, Aug. (1993)
10. Mallat, S.G.: A theory of multiresolution signal decomposition: The wavelet representation. IEEE Trans. Patt. Anal. Mach. Intell., vol. 11, no. 7, pp. 674-693 (1989)
11. Tanaka, K., Carlier, S. G., Katouzian, A., Mintz, G.: Characterization of the intravascular ultrasound radiofrequency signal within regions of acoustic shadowing behind calcium. J. Am. Coll. Cardiol., vol. 49, no. 9, Suppl. B, 29B (2007)